Modeling of Equiaxed Microstructure Formation in Casting

Ph. THÉVOZ, J.L. DESBIOLLES, and M. RAPPAZ

A general micro/macroscopic model of solidification for 2-D or 3-D castings, valid for both dendritic and eutectic equiaxed alloys, is presented. At the macroscopic level, the heat diffusion equation is solved with an enthalpy formulation using a standard FEM implicit scheme. However, instead of using a unique relationship between temperature and enthalpy (*i.e.*, a unique solidification path), the specific heat and latent heat contributions, whose sum equals the variation of enthalpy at a given node, are calculated using a microscopic model of solidification. This model takes into account nucleation of new grains within the undercooled melt, the kinetics of the dendrite tips or of the eutectic front, and a solute balance at the scale of the grain in the case of dendritic alloys. The coupling between macroscopic and microscopic aspects is carried out using two time-steps, one at the macroscopic level for the implicit calculation of heat flow, and the other, much finer, for the microscopic calculations of nucleation and growth. This micro/macroscopic approach has been applied to one-dimensional and axisymmetric castings of Al-7 pct Si alloys. The calculated recalescences and grain sizes are compared with values measured for one-dimensional ingots cast under well-controlled conditions. Furthermore, the influence of casting conditions on temperature field, undercooling, grain size, and microstructural spacings is shown to be predicted correctly from axisymmetric calculations with regard to the expected experimental behavior.

I. INTRODUCTION

MICROSTRUCTURE formation during the solidification of alloys is of prime importance for the control of the properties and quality of cast products. In order to predict the properties and the soundness of a casting, empirical methods or trial approaches have been used over the last decades. However, due to the complex interactions occurring during solidification, these methods have a rather limited use and hardly can be extended to other solidification conditions. Furthermore, they usually give little insight into the basic mechanisms of solidification. This is particularly the case in equiaxed microstructure formation where nucleation, growth kinetics, solute diffusion, and grain interactions have to be considered simultaneously with heat diffusion. For these reasons, the modeling of solidification using powerful numerical techniques and consideration of the basic mechanisms of microstructure formation are becoming important fields of development.

Since the pioneering work of Murray[1] in 1959 concerning heat flow calculations, most of the effort expended in modeling of casting processes has been focused on the macroscopic scale. Energy, mass, momentum, and/or solute continuity equations have been used to calculate temperature fields,[2] mold filling,[3] convection,[4] or macrosegregation.[5] Developments also have been directed toward geometric modeling to handle complex two- or three-dimensional geometries. Macroscopic calculations provide interesting information about macro-defects due to insufficient feeding, holes, hot spots, hot tearing, and macroporosity, as well as columnar microstructural parameters deduced from the isotherms. However, these heat flow calculations, using simplified models to handle the phase change, cannot predict the microstructural parameters of equiaxed structures, such as grain size, eutectic or dendritic spacing, volume fraction of each phase, or solidification morphology.

The first attempt to couple the microscopic aspects of solidification with the continuity equation of energy was made in 1966 by Oldfield[6] for gray cast iron. As a matter of fact, most of the work done in this area since 1966 deals with eutectic alloys.[7,8,9] This case, indeed, is much simpler than that of dendritic alloys since the eutectic grains are fully solid. Maxwell and Hellawell[10] have considered the various mechanisms of nucleation and growth of equiaxed dendritic grains in order to analyze the cooling curve, near to recalescence, of a small ingot of uniform temperature. However, they performed their analysis by making the assumption that the dendritic grain was a solid sphere. Dustin and Kurz[11] relaxed this assumption by setting the internal volume fraction of the solid within the dendritic grain equal to a fixed value, different from unity. When analyzing the columnar to equiaxed transition, Flood and Hunt[12,13] integrated a microscopic model of equiaxed dendritic growth into a simplified one-dimensional calculation of the heat flow. However, their microscopic model did not consider solute diffusion outside of the grain envelope.

The present paper describes a new and general approach to the micro/macroscopic modeling of equiaxed dendritic solidification, the aim being to remove most of the limitations of the previous models. Although this work is focused mainly on dendritic solidification, it can be applied to eutectic alloys as well. At the macroscopic scale, the model is based upon a heat flow calculation, neglecting convection within the melt. As described in Section II, the heat diffusion problem is solved using a Finite Element Method (FEM), involving an enthalpy formulation and an implicit scheme.[14] At the microstructural scale, formation of equiaxed dendritic grains

Ph. THÉVOZ and J.L. DESBIOLLES, Staff Members, and M. RAPPAZ, Group Leader, are with the École Polytechnique Fédérale de Lausanne, Département des Matériaux, Laboratoire de Métallurgie Physique, 34 Chemin de Bellerive, CH-1007 Lausanne, Switzerland.

Manuscript submitted February 15, 1988.

(Section III) is calculated according to a nucleation model[15] and to a growth model which considers the kinetics of the dendrite tips and solute diffusion at the scale of the grain.[16,17] Coupling between the macroscopic calculation of heat flow and the microscopic calculation of the nucleation and growth of equiaxed crystals (Section IV) is achieved using a newly-developed scheme which is based upon two different time-steps: a fairly large time-step for the implicit FEM calculation of heat flow and a much finer one for the calculation of nucleation and growth. This two time-steps procedure reduces the computing time, thus permitting the handling of forms with complex geometry in two or three dimensions. The results obtained from this micro/macroscopic model of solidification (Section V) are compared with the cooling curves and grain sizes measured for well-controlled one-dimensional castings of Al-7 pct Si alloy. The influence of casting conditions upon the temperature field and upon the final microstructure also are emphasized in the case of axisymmetric castings.

II. MACROSCOPIC MODEL

In order to analyze microstructure formation in castings, one has to know the temperature field at each time-step. This is achieved by using the macroscopic model described below.

Neglecting convection in the liquid zone, the temperature field obeys the nonstationary heat flow equation:

$$Div\,(\kappa(\mathbf{x},T)\ \mathbf{grad}\ T(\mathbf{x},t)) = c_p(\mathbf{x},t)\frac{\partial T(\mathbf{x},t)}{\partial t} - L\cdot\frac{\partial f_s(\mathbf{x},t)}{\partial t} \qquad [1]$$

where κ is the thermal conductivity, c_p is the volumic specific heat, L is the volumic latent heat of fusion, and T and f_s are the temperature and solid fraction fields, respectively.

The term on the right-hand side of Eq. [1] represents the variation in enthalpy at a given point of the casting, the enthalpy being defined as:

$$H(T) = \int_0^T c_p(T')\,dT' + L\cdot(1 - f_s) \qquad [2]$$

In a standard macroscopic approach, the fraction of solid, f_s — and, accordingly, the enthalpy, H — will be considered to be only temperature-dependent by using, for example, a Scheil or Brody-Flemings model of solute diffusion.[18] In a more general approach, the enthalpy also can be a function of time, cooling rate, grain density, *etc.* However, for a given heat flow, Eq. [1] states that the variation in enthalpy is independent of the solidification path. Therefore, it might be advantageous at the macroscopic scale to choose enthalpy as the variable rather than temperature. One then can write:

$$Div(\kappa(\mathbf{x},T(H(\mathbf{x},t)))\ \mathbf{grad}\ T(H(\mathbf{x},t))) = \frac{\partial H(\mathbf{x},t)}{\partial t} \qquad [3]$$

This enthalpy formulation offers several advantages. First, any discontinuity associated with a sharp phase transformation is removed. Second, energy can be conserved without taking special care as in the equivalent-specific-heat method. Third, during cooling, any solidification path is characterized by a strictly decreasing enthalpy. This latter point is very important, especially during recalescence, as will be emphasized later.

The solution of Eq. [3] for arbitrary geometries can be obtained only using numerical methods. Among existing techniques, the Finite Element Method (FEM) is probably the best suited to the handling of complex shapes (Figure 1) with a limited number of nodes, and it was chosen here for that reason. The classical Galerkin formulation of Eq. [3] for the FEM gives the following set of nonlinear equations:

$$-[K]\cdot\{T(H)\} + \{b\} = [M]\cdot\frac{\partial\{H\}}{\partial t} \qquad [4]$$

where $[M]$ is the mass matrix, $[K]$ is the conductivity matrix, $\{b\}$ is the vector of boundary conditions, and $\{T\}$ and $\{H\}$ are the vectors of temperature and enthalpy, respectively, at each node of the mesh. In the enthalpy formulation, note that the specific heat, c_p, does not appear explicitly in Eq. [3]. Therefore, the mass matrix $[M]$ is constant and can be calculated only once since the temperature-dependent specific heat and the latent heat terms have been incorporated into the enthalpy.

The time discretization is performed using an Euler implicit scheme. In that case, there is, in principle, no

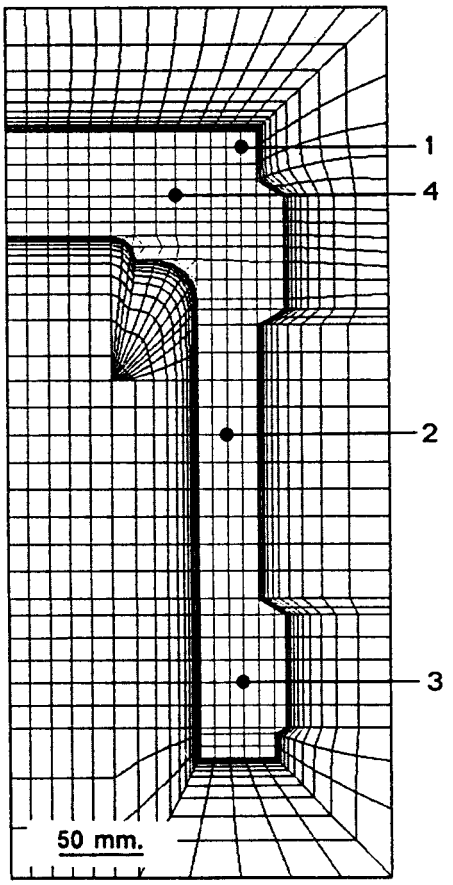

Fig. 1—Mesh of an axisymmetric casting used in the Finite Element (FEM) program, 3-MOS. The left vertical edge of the mesh corresponds to the axis of revolution.

limitation on the choice of the time-step, unlike explicit methods where time-steps are limited by a stability criterion. If one assumes that the conductivity matrix, $[K]$, and the boundary condition term, $\{b\}$, are not varying too dramatically with time, then the system of equations (Eq. [4]) can be written as:

$$[M]\cdot\frac{\{\Delta H\}}{\Delta t}+[K]^t\cdot\{T\}^{t+\Delta t}=\{b\}^t \qquad [5]$$

where $\{\Delta H\}$ is the vector of the variation in enthalpy at each node during the time-step, Δt. The upper index indicates the time at which the variables, or the matrices, are taken.

The temperature-enthalpy relationship is linearized using Newton's method, restricted to the first iteration. This is equivalent to write:

$$\{T\}^{(t+\Delta t)}=\{T\}^t+\left[\frac{\partial T}{\partial H}\right]^t\cdot\{\Delta H\} \qquad [6]$$

where $[\partial T/\partial H]$ is the diagonal matrix of the derivative $\partial T/\partial H$ at each node. In the case of a standard macroscopic approach of solidification, these values can be obtained readily by deriving the relationship, $T(H)$, given by Scheil's equation, for example. In the micro/macroscopic approach which is presented, the slope $\partial T/\partial H$ at each node was set to $1/c_p$.* (This prevents some oscillations which might occur near recalescence, while keeping an overall energy balance.) The absence of further iterations is justified as long as the time-step is sufficiently small with respect to the total solidification time. However, this physical limitation is less severe than the one imposed by an explicit scheme.

*It was verified in pure macroscopic calculations that the replacement of $\partial T/\partial H$ by $1/c_p$ during solidification does not induce any significant differences in the cooling curves.

Combining Eqs. [5] and [6] gives:

$$\left[\frac{1}{\Delta t}\cdot[M]+[K]^t\cdot\left[\frac{\partial T}{\partial H}\right]^t\right]\cdot\{\Delta H\}=-[K]^t\cdot\{T\}^t+\{b\}^t \qquad [7]$$

The set of equations (Eq. [7]) is solved for $\{\Delta H\}$ using the direct triangulation method of Gauss. In the context of a macroscopic calculation only, the knowledge of the new enthalpy, $H_j^t+\Delta H_j$, of each node, j, permits us to calculate the new temperature, using the unique relationship, $T(H)$ (Eq. [2]). Thus, from the initial conditions, it is possible to know, step-by-step, the evolution of the temperature field. In the case of micro/macroscopic coupling, the iterative procedure is somewhat similar. However, once the variation in enthalpy during one time-step, Δt, is known at each node, the conversion to temperature is not achieved using $T(H)$ (Eq. [2]), but using the microscopic calculation of nucleation and growth presented in the next section.

A computer program named 3-MOS (Micro-Macroscopic Modeling Of Solidification) was written in order to solve this problem. This program uses some routines from the FEM library MODULEF,[19] and includes a solver, as well as pre- and post-processing modules (mesh generation, input data processing, interactive color graphics presentation of results, and so forth). Any two-dimensional or axisymmetric geometries involving several different media (metal, mold, and chill) can be treated under various boundary conditions (Dirichlet, Neumann, and Cauchy), which can be time-, space-, and temperature-dependent.

During solidification, an air gap can form between mold and metal, thus invalidating the assumption of perfect thermal contact between these two media. In order to introduce a heat-transfer coefficient between them, a special coupling element of zero width[20] has been developed. Two degrees of freedom for the nodes located at the given interface are allowed, the temperatures of which are related by the condition:

$$\kappa_1(T_j^{(1)})\frac{\partial T_j^{(1)}}{\partial n}=\kappa_2(T_j^{(2)})\frac{\partial T_j^{(2)}}{\partial n}=h\cdot(T_j^{(2)}-T_j^{(1)}) \qquad [8]$$

where κ_1 and κ_2 are the thermal conductivities of media 1 and 2, respectively; $\partial T/\partial n$ is the temperature derivative along the outward normal, $\mathbf{n}$, to the interface of medium 1, $T_j^{(m)}$ is the temperature of medium m at the node j, and h is a given heat transfer coefficient.

III. MICROSCOPIC MODEL

A. *Introduction*

Equiaxed solidification involves various phenomena which have to be taken into account simultaneously. First, nucleation occurs in an undercooled melt. Second, as soon as a nucleus appears, it grows. This growth is controlled by the thermal and solute fields and by surface effects. Finally, when the grains are large enough, they will interact *via* their thermal or solute layers. The aim of the microscopic model is to combine nucleation, grain growth, and grain interaction in order to have a full description of equiaxed solidification.

Under solidification conditions usually encountered in castings, microstructure formation in alloys is controlled mainly by solute diffusion and by capillarity effects. Accordingly, thermal diffusion can be neglected at the microscopic scale (*i.e.*, complete thermal mixing at the microstructure scale). Consider a small volume, V, of uniform temperature corresponding to one mesh in a casting (Figure 1) or to a sample in a DTA-type experiment. The heat flow, Q_{ext}, leaving the surface, S, of that volume element can be related directly to the change in volumic enthalpy, ΔH, during the time-step, Δt. One has:

$$Q_{ext}\cdot\frac{S}{V}\cdot\Delta t=\Delta H=c_p\Delta T-L\Delta f_s \qquad [9]$$

In equiaxed dendritic growth, the solid fraction, f_s, can be written as:[17]

$$f_s(t)=n(t)\cdot\frac{4}{3}\pi R^3(t)\cdot f_i(t) \qquad [10]$$

where $n(t)$ is the grain density, $R(t)$ is the mean radius of the spherical envelope of the grain, and $f_i(t)$ is the internal solid fraction which corresponds to the fraction

of solid within the spherical envelope of the crystal. Although the grain density, $n(t)$, is updated at each time-step according to a nucleation model, its contribution, $\Delta n(t)$, can be neglected when deriving Eq. [10]. Therefore, one gets:

$$\Delta f_s(t) = n(t) \cdot \left(4\pi \cdot R^2(t) \cdot \Delta R(t) \cdot f_i(t) + \frac{4}{3} \pi \cdot R^3(t) \cdot \Delta f_i(t) \right) \qquad [11]$$

where $\Delta R(t)$ is the increase in the radius of the spherical envelope of the equiaxed grain and $\Delta f_i(t)$ is the variation in the internal solid fraction.

In order to solve the problem, one must know how $n(t)$, $R(t)$, and $f_i(t)$ change with time. The grain density, $n(t)$, is calculated according to a nucleation model[15] as shown in Section III–B, while $R(t)$ and $f_i(t)$ are given by an analytical solute diffusion model for equiaxed dendritic growth, recently proposed by Rappaz and Thévoz[17] and briefly summarized in Section III–C.

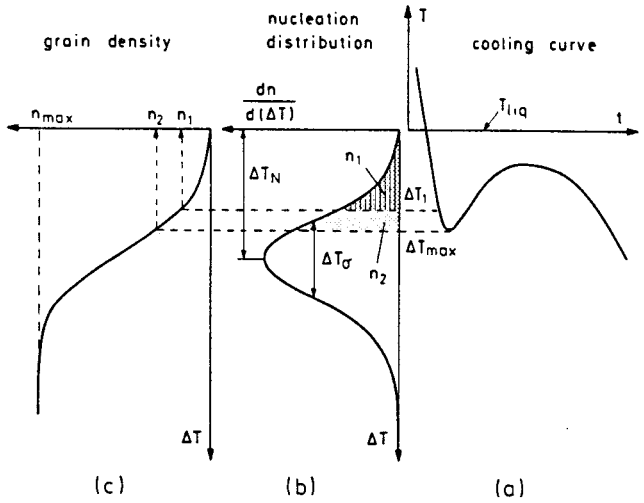

Fig. 2—Nucleation model used in the microscopic calculation of equiaxed solidification. At a given undercooling (a), ΔT_1, the density of nuclei, n_1, within the liquid is given by the integral (c) of the distribution (b).

B. *Nucleation Model*

Most of the work done on micro/macroscopic modeling[10–13] uses a heterogeneous nucleation law with an extinction factor[21] to halt nucleation. However, at low undercooling, the range of undercooling within which the density of grains goes from zero to the maximum value, n_0, is so narrow that it is difficult to reproduce experimental observations. The final grain density is always equal to the maximum value, n_0, regardless of the cooling rate. On the other hand, experimental observations[22] have shown that different inoculant particles can become active at different undercoolings. These two observations provided the incentive to develop a new nucleation model,[15,23] based upon a distribution of nucleation sites, each becoming active at different undercoolings.

Figure 2 summarizes this nucleation model. At a given undercooling, ΔT_1 (Figure 2(a)), the grain density is given by the integral of the nucleation site distribution from zero undercooling to ΔT_1 (Figure 2(b)). As Figure 2(c) represents the integral of the nucleation distribution, the grain density, n_1, corresponding to ΔT_1, can be obtained directly. By this means, the new grain density is updated at each time-step as a function of the undercooling. When the minimum in the cooling curve is reached, *i.e.*, when recalescence occurs, this corresponds to the final grain density, n_2, associated with the maximum undercooling, ΔT_{max}.

As for the heterogeneous nucleation law, which is defined by three parameters, the nucleation distribution also can be characterized by two or three parameters, depending upon the distribution function being used. If the distribution of nuclei is approximated by a gaussian distribution, for example, one can define the mean nucleation undercooling, ΔT_N, corresponding to the maximum of the distribution, the standard deviation of the distribution, ΔT_σ, and the maximum density of nuclei, n_{max}, given by the integral of the total distribution (from zero undercooling to infinite undercooling). These three parameters can be determined experimentally for each melt by measuring the grain density (*i.e.*, the grain size) and the corresponding maximum undercooling at recalescence, ΔT_{max}, under various cooling conditions. Then, an error function can be fitted to these measured $n - \Delta T_{max}$ points (Figure 2(c)).

C. *Growth Model*

The aim of the growth model is to calculate the average grain radius, $R(t)$, and the internal volume fraction of solid, $f_i(t)$, as a function of time (Eq. [11]). A model based on solute diffusion[16,17] provides the relationships between these unknowns, and the temperature and time. The basic hypotheses of the solute diffusion model are (1) rapid thermal diffusion at the scale of the grain; *i.e.*, the temperature is uniform and equal to the dendrite tip temperature, T^*; (2) the interdendritic liquid, where complete mixing of solute is achieved, extends to the spherical envelope of the grain; (3) the spherical solute diffusion layer outside of the grain envelope is replaced by a solute boundary layer, δ, of unknown thickness; (4) an overall solute and thermal balance is satisfied at the scale of the grain. The main result of the model is that it can relate the internal volume fraction of solid, f_i, to the supersaturation,* Ω, *via* the relationship:

*$\Omega = (c^* - c_0)/(c^* \cdot (1 - k)) \simeq (c^* - c_0)/(c_0 \cdot (1 - k))$ for low undercooling. c^* is the concentration of the liquid at the dendrite tip; c_0 is the initial concentration of the alloy; and k is the partition coefficient.

$$f_i = \Omega \cdot f(\mathrm{Pe}) \qquad [12]$$

where Pe is the Péclet number of the grain.* The correction factor, f(Pe), in Eq. [12] appears when the solute boundary layer, δ, is considered. By applying a solute

*$\mathrm{Pe} = v \cdot R/2D$ where v is the dendrite tip velocity, R is the radius of the grain, and D is the solute diffusion coefficient in the liquid.

flux balance at the grain boundary, R, one can show that this boundary layer, δ, is given by that of a planar front, *i.e.*, $\delta = 2 \cdot D/v$.

Assuming that d/dt (f(Pe)) is small with respect to $d\Omega/dt$, one has:

$$\frac{df_i}{dt} \approx \frac{d\Omega}{dt} \cdot f(\text{Pe}) = \frac{f(\text{Pe})}{c_0 \cdot (1-k)} \cdot \frac{dc^*}{dt}$$

$$= \frac{f(\text{Pe})}{mc_0 \cdot (1-k)} \cdot \frac{dT^*}{dt} \qquad [13]$$

where m is the slope of the liquidus line. It appears from Eq. [13] that the variation in the internal solid fraction, Δf_i, in Eq. [11] can be related to the variation in temperature.

On the other hand, the position of the dendrite tips which gives the grain radius, R, is such that:

$$\Delta R = v \cdot \Delta t = v(\Delta T) \cdot \Delta t \qquad [14]$$

where v is the growth velocity of a free dendrite tip in an undercooled melt as deduced, for example, from the model of Lipton *et al.*[24] If one neglects the thermal and curvature undercoolings, which are very small for metallic alloys, v is a function only of the solute undercooling of the dendrite tip, *i.e.*, of the difference between the liquidus temperature, T_{liq}, and the grain temperature, T.

It should be pointed out that, when the diffusion layer of the grain, δ, starts to interact with the layers of neighboring grains, the concentration at the grain boundary will be increased, thus slowing down the dendrite tips. The solute balance made at the scale of the grain can account for this last stage of grain growth, as shown in Reference 17. At this stage, a state of nearly complete solute mixing is reached, and the solute model resumes to Scheil's equation.[18]

By coupling Eqs. [11], [12], [13], and [14], and grouping the terms, one gets:

$$\Delta f_s = A \cdot (T^{t+\Delta t} - T^t) + B \cdot v(\Delta T^t) \cdot \Delta t \qquad [15]$$

The first term represents the contribution made by the change in internal solid fraction, Δf_i, which depends in turn upon the variation of temperature with time (Eq. [13]). The second term is the contribution made by the volume increase of the grain as governed by the kinetics of the dendrite tip. A and B in Eq. [15] are not constants, but functions of $n(t)$, $R(t)$, $T(t)$, and Pe(t) and must be calculated at each time-step and each node.

IV. COUPLING (MICROENTHALPY MODEL)

Provided that the heat flow coming out of a small volume element is given, the enthalpy change of the solidifying alloy is independent of the solidification path. However, the heat flow itself within a casting is dictated by the temperature distribution and, thus, varies slightly with the solidification conditions. In an implicit scheme, the temperature field and the associated heat flow are taken at time, $t + \Delta t$, and therefore are not known explicitly. Accordingly, the linearization procedure (Eq. [6]) in principle should be iterated until the micro/macroscopic coupling has converged to consistent values of both temperature and enthalpy.* However, for a given computing time, more accurate results can be obtained if only one iteration is made and the time-step is reduced accordingly.

*For a given value of enthalpy change, ΔH_j, the variation, ΔT_j, calculated using the microscopic model of solidification (Section III) can vary, depending upon the solidification conditions, from the value associated with simple cooling: $\Delta f_{s_j} = 0$ and $\Delta T_j = \Delta H_j/c_p$ to that characterizing an isenthalpic reaction: $\Delta H_i = 0$ and $\Delta T_j = \Delta f_{s_i} \cdot L/c_p$.

Figure 3 shows a flow chart of the micro/macroscopic enthalpy-based coupling which was used. For the sake of simplicity, the preprocessing modules (enmeshment,

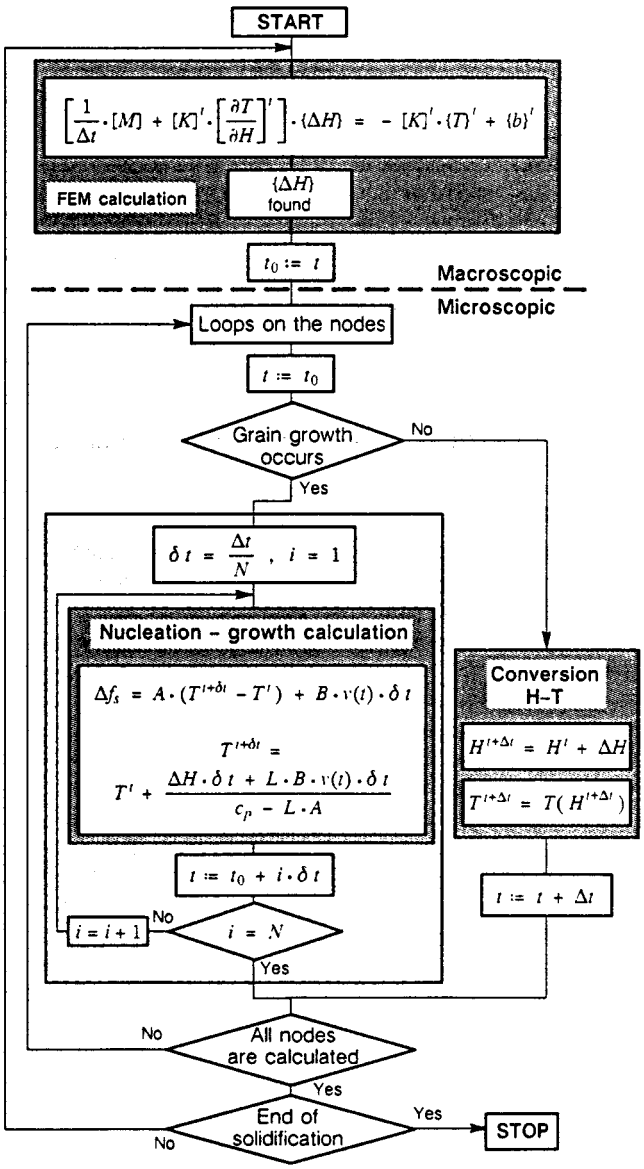

Fig. 3—Flow chart of the micro/macroscopic enthalpy-based model of equiaxed solidification; at the macroscopic level, the variation in enthalpy at each node of the mesh is calculated using the enthalpy as the variable in a FEM formulation. This variation in enthalpy is then converted into specific heat and latent heat contributions using the microscopic model of equiaxed solidification.

input of physical data, of boundary conditions, and of initial conditions) as well as the post-processing ones (graphics presentation of results) are not displayed on this flow chart. It is first assumed that the integer, N, which divides the time-step, Δt, is equal to one. Therefore, the variation in enthalpy at each node, ΔH_j, calculated from the implicit FEM scheme (Section II) is converted, in a single operation, into a temperature change, ΔT_j, and a solid fraction variation, Δf_{s_j}, using a microscopic model of solidification described in Section III. Although the implicit scheme is not subject to a stability criterion, the time-step in this case has to be kept small enough so as to go through the recalescence stage in many steps. In other words, the choice of time-step is imposed primarily by the physical phenomena and not by the mathematics of the numerical method. For high cooling rates, *i.e.*, for meshes close to a chill, the time increment required to describe recalescence carefully (100 steps, for instance) may be much smaller than the explicit time-step. This makes the implicit scheme no longer favorable, at least when calculating microstructure formation.

However, as shown in the flow chart (Figure 3), the macroscopic calculation of the enthalpy variations, $\{\Delta H\}$, is separated from the microscopic routines which predict $\{\Delta T\}$ and $\{\Delta f_s\}$. Assuming that the enthalpy change rate, dH_j/dt, is constant during one time-step, $\Delta t = \Delta t_{macro}$, and is given by $\Delta H_j/\Delta t$, the nucleation and growth can be calculated using a much finer time-step, $\delta t = \Delta t/N = \delta t_{micro}$, while retaining a fairly large time-step for the macroscopic calculation of heat flow. Thus, the solidification path is split into N microscopic time-steps, δt, according to Eq. [9], where ΔH_j is replaced by $\delta H_j = \Delta H_j/N$. This corresponds to adding a loop to the flow chart ($N > 1$ in Figure 3).

Figure 4 summarizes this two time-steps procedure. The method permits the calculation of nucleation and growth using very fine time-steps, so as to carefully describe recalescence, while keeping a large time-step for the macroscopic calculation of heat flow. Since fine time-steps are needed only for those meshes which are in the nucleation or the growth stages, computing times are reduced greatly in comparison with micro/macroscopic calculations using a single time-step procedure.

On the other hand, another phenomenon, which the present authors have called the *bouncing effect*, can be eliminated by means of the two time-steps procedure. Bouncing of cooling curves on one another often is observed in heat flow calculations when cooling curves exhibit sudden changes in the first derivative (*e.g.*, at the eutectic plateau or when recalescence occurs). This numerical phenomenon can be explained as follows. When one mesh, j, recalesces, it still is characterized by a negative variation of the enthalpy, ΔH_j, although its temperature, T_j, is increasing. This sudden temperature increase can reverse the local thermal gradient and cause reheating of neighboring meshes ($\Delta T_j > 0$ with $\Delta H_j > 0$). This reheating is similar to the wiggles observed when calculating the solidification of a eutectic alloy.[25] In the latter case, the cooling rates of nodes close to solidifying meshes are slowed down, thus inducing *false* eutectic plateaus in the cooling curves. Both reheating or false eutectic plateaus have no real significance as they would not appear in a continuous model, *i.e.*, when the mesh size and the time-step used in FEM calculations tend to zero.

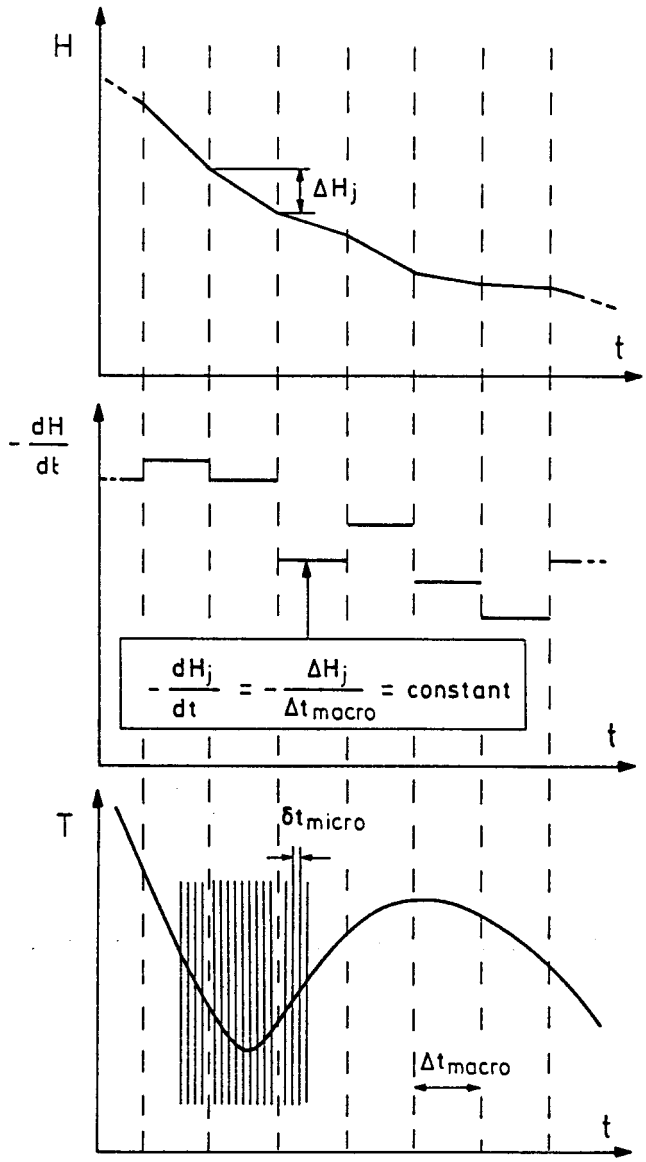

Fig. 4—Illustration of the two time-steps procedure. During the time-step, Δt, dH_j/dt is kept constant and equal to $\Delta H_j/\Delta t$.

Unlike the wiggles appearing in standard calculations of eutectic solidification, reheating of neighboring meshes not only disturbs the presentation of cooling curves but also modifies the calculation of nucleation and growth close to the liquidus temperature. As will be shown below, a micro/macroscopic scheme based upon two time-steps (Figures 3 and 4) permits one to avoid this reheating phenomenon and thus ensure good convergence of the results.

V. RESULTS

The micro/macroscopic enthalpy-based model was applied to Al-7 pct Si alloy solidifying with an equiaxed dendritic morphology. Calculations were performed for 1-D and axisymmetric geometries using the program 3-MOS.

A. *One-Dimensional Castings*

The results of a one-dimensional calculation, using the parameters listed in Table I, is presented first in Figure 5. The cooling curves correspond to the locations indicated in the upper part of the figure. These cooling curves show that, near the recalescence stage, each volume element is independent, more or less, of the neighboring ones, and no bouncing or reheating effect is observed. As shown hereafter, convergence of the method is nearly assured by this coupling.

In order to test the convergence of the micro/macroscopic enthalpy-based coupling, the cooling curves of Figure 5 were calculated using seven different mesh sizes (0.6, 0.8, 1.2, 2, 3, 6, and 12 mm) and five different time steps, Δt (0.1, 0.5, 1, 2, and 4 seconds). The maximum undercooling of the cooling curves near to recalescence, ΔT_{max}, is plotted *vs* the number of meshes (or mesh size) (Figure 6(a)) and *vs* Δt (Figure 6(b)) for the same locations corresponding to the nodes labeled 2, 4, 6, 8, and 10 in Figure 5. The triangles correspond to the values of Figure 5. It can be seen in Figure 6(a) that the convergence with mesh size is excellent, except for too large mesh (shaded area). Such good convergence was not obtained using a single time-step method because of bouncing effects. As far as the influence of the time-step is concerned (Figure 6(b)), convergence is obtained only within a given range of Δt values. When too small time-steps are used, bouncing of cooling curves occurs (shaded area 1), and no convergence is obtained. For Δt values between 0.5 and 2.5 seconds, convergence is good; the undercooling increases slightly with Δt because the absence of iteration at the macroscopic level leads to an overestimation of the heat flow when the slope, $(\partial T/\partial H)_j$, at a given node, j, suddenly decreases at recalescence (*i.e.*, numerical diffusion is introduced). When Δt becomes too large with respect to the recalescence time, numerical diffusion becomes too important, and the results diverge (shaded area 2). Finally, convergence with the time step, δt, used in the microscopic calculations is not a problem as long as it is kept sufficiently small with respect to the microscopic phenomena (typically 0.005 to 0.01 seconds in all of the calculations on Al-7 pct Si).

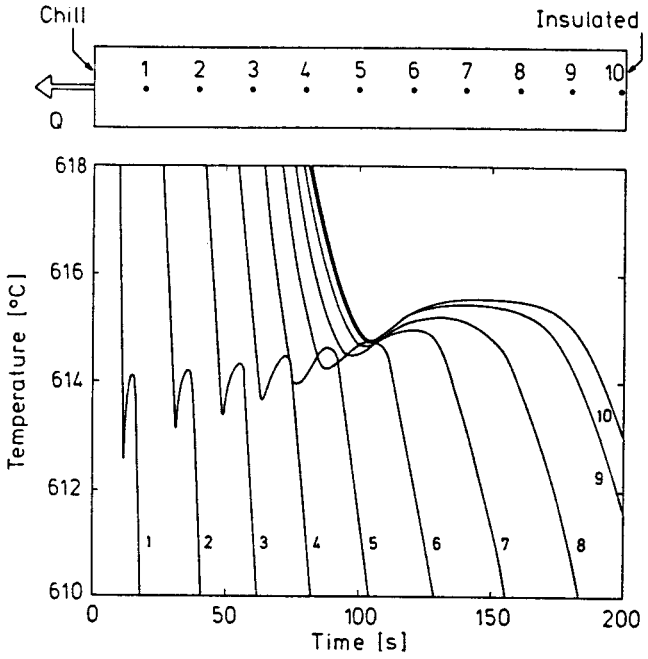

Fig. 5—Cooling curves for a 1-D casting of Al-7 pct Si (T_{liq} = 618 °C). The curves correspond to the locations indicated at the top of the figure. The difference between T_{liq} and the minimum of the cooling curve near the recalescence is defined as the maximum undercooling, ΔT_{max}.

Figures 7 and 8 compare the results of numerical simulation with measurements made on one-dimensional castings. Al-7 pct Si alloy, inoculated with 50 ppm of Ti, was poured into a cylindrical ceramic mold with a water-cooled copper chill plate at the bottom. The almost one-dimensional heat flow obtained using this geometry was deduced from the temperatures recorded by

Table I. List of Parameters

Alloy Characteristics (Al-Si):				
c_0	=	7	[pct]	alloy concentration (wt pct)
m	=	−6	[K pct^{-1}]	liquidus slope
k	=	0.13	[−]	partition coefficient
D	=	$3 \cdot 10^{-9}$	[m^{2}s^{-1}]	liquid diffusion coefficient
a_2	=	$2.904 \cdot 10^{-6}$	[m·s^{-1}·K^{-2}]	kinetic coefficient (Eq. [17])
a_3	=	$1.488 \cdot 10^{-6}$	[m·s^{-1}·K^{-3}]	kinetic coefficient (Eq. [17])
L	=	$9.5 \cdot 10^{8}$	[J·m^{-3}]	volumic latent heat of fusion
c_p	=	$2.6 \cdot 10^{6}$	[J·m^{-3}·K^{-1}]	average volumic specific heat
κ	=	90	[W·m^{-1}·K^{-1}]	average thermal conductivity
M	=	$8.8 \cdot 10^{-6}$	[m·s$^{-1/3}$]	coarsening factor (Eq. [18])
Inoculation (Ti):		50	[ppm]	Ti-base inoculant

Calculation Parameters:		Figure 5	Figures 7 through 8	Figures 9 through 12
Number of meshes	[−]	100	60	1139
Δt	[sec]	1	1	1
δt	[sec]	0.01	0.01	0.005
ΔT_N	[K]	6	4	6
ΔT_σ	[K]	1	1	1
n_{max}	[m^{-3}]	10^9	10^{11}	10^{11}
Initial temperature	[°C]	720	720	650

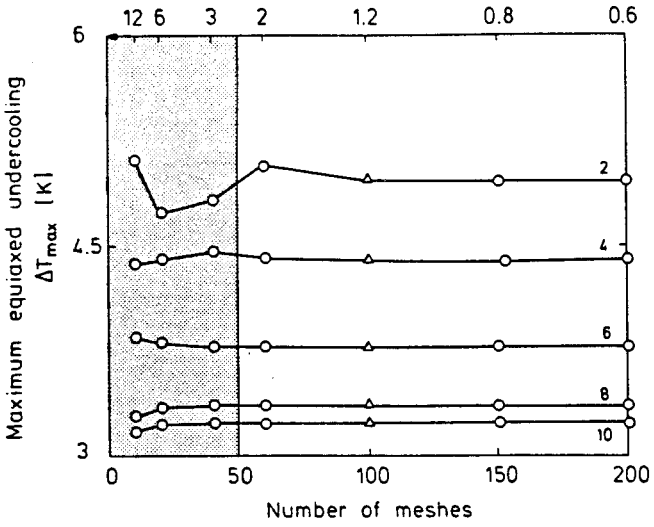

(*a*)

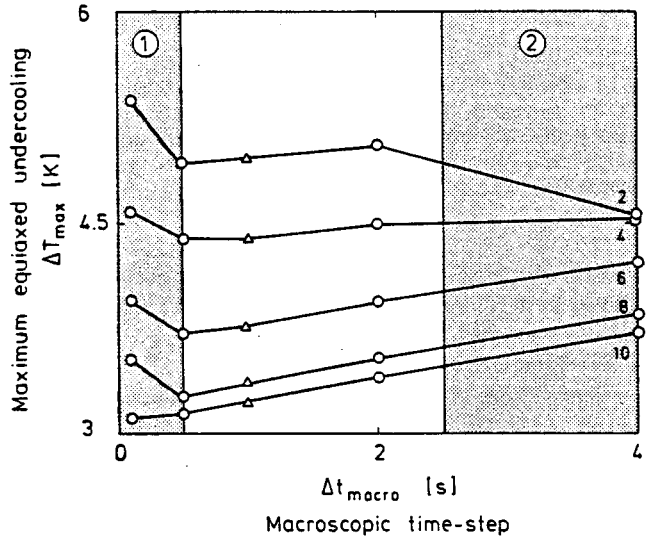

(*b*)

Fig. 6—Convergence of the micro/macroscopic model. Maximum undercooling, ΔT_{max}, of the equiaxed microstructure *vs* (*a*) number of meshes; (*b*) macroscopic time-step, Δt. Triangles are for the values corresponding to Fig. 5.

thermocouples placed within the chill.[23] Five thermocouples within the casting itself, positioned at 20, 40, 60, 80, and 100 mm from the chill plate, permitted the recording of cooling curves during solidification. The initial temperatures of the melt and ceramic mold were 720 and 150 °C, respectively. After solidification, the cylindrical ingot was cut longitudinally, and metallographic sections of the five regions near the thermocouples were prepared by polishing and etching with Barker's solution. The average grain radius, R, was then deduced from the quantitative measurement of the surface density of the grains, N_A, and of the mean linear intercept, N_L, using the relationship normally valid for a random arrangement of spheres:[26]

$$R = \frac{2N_L}{\pi N_A} \qquad [16]$$

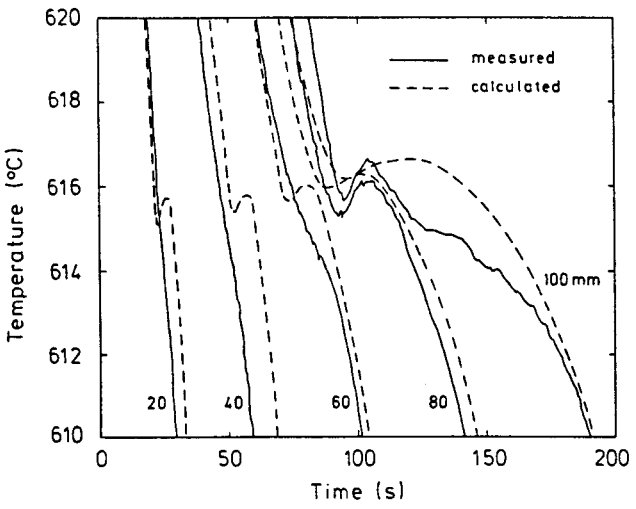

Fig. 7—Measured and calculated cooling curves for a 1-D casting of Al-7 pct Si inoculated with 50 ppm of Ti (T_{liq} = 618 °C). The measured curves correspond to thermocouples located at 20, 40, 60, 80, and 100 mm from a water-cooled copper chill plate. The parameters used in the calculation are listed in Table I.

The cooling curves recorded by the five thermocouples are shown in Figure 7, and the corresponding grain radii are plotted *vs* the distance from the chill plate in Figure 8. The calculated cooling curves and grain radii, which are shown in the same figures, were obtained using the parameters listed in Table I. It should be pointed out that the kinetics of the dendrite tip (Eq. [14]) was that given by the model of Lipton *et al.*,[24] neglecting thermal and curvature undercoolings. No adjustable parameter was introduced at this stage. In order to speed up the calculations, the kinetic law obtained using this model was described by a polynomial law, which fits Lipton's model:

$$v(\Delta T) = a_2 \cdot \Delta T^2 + a_3 \cdot \Delta T^3 \qquad [17]$$

where ΔT is the undercooling, and a_2 and a_3 are given in Table I.* The only free parameters which have to be

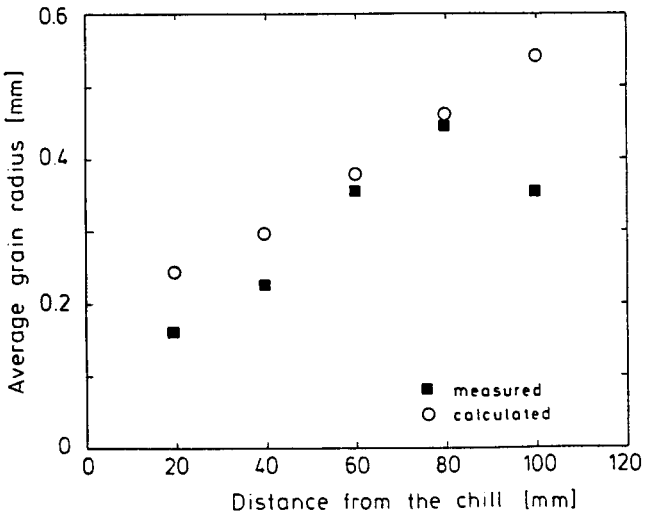

Fig. 8—Calculated and measured grain radii for the Al-7 pct Si 1-D casting whose cooling curves are shown in Fig. 7.

*Note that a quadratic kinetic law is obtained using a simpler analysis of dendrite tip growth[18] and that this law has been used in recent papers on the modeling of the growth of equiaxed dendritic grains.[16,17] However, substantial differences (a factor 3 to 8) occur between this quadratic kinetic law and the result of the full analysis of Lipton *et al.* (Eq. [17]). The slowing factor introduced in the kinetic law of previous papers[16,17] no longer is used in the present calculations.

defined are those associated with the nucleation law (Figure 2). The three parameters of the gaussian shape characterizing the nucleation site distribution were deduced using the procedure described in Section III–B. These values are listed in Table I.

As can be seen, it is possible, using only three parameters, to obtain a good agreement between calculated and measured grain sizes (Figure 8), especially if one considers the difficulty of defining and measuring the average radius of equiaxed dendritic grains in a micrograph. (It should be pointed out that grain sizes were measured independently at the Max Planck Institute, Stuttgart.) The larger discrepancy observed for the point farthest from the chill (100 mm) may be due to convection effects, as these are not taken into account in the model and will become more marked at low thermal gradients.

As far as agreement between the cooling curves is concerned (Figure 7), the depth and width of the recalescences calculated for curves 4 and 5 (thermocouples at 80 and 100 mm from the chill) are close to the measured ones. For the other three curves, no recalescence is measured, while the model, indeed, predicts that recalescence occurs at those points. This may be due to various causes; the thermocouple response time may be too large with respect to the recalescence period of these curves. As fine platinum wires (0.2 mm diameter) with a thin ceramic coating were used, this effect is certainly of minor importance. More important is the volume sensed by the thermocouples. In a thermal gradient, the measured temperature is a convolution of various regions which may recalesce at different times. But, most importantly, the assumption of a uniform temperature of the mesh at the microscopic level is no longer valid. When the temperature difference across the dendritic grain (*i.e.*, a value equal to the grain size multiplied by the thermal gradient) is larger than the depth of the recalescence calculated using the model, the recalescence is smeared out.

B. *Axisymmetric Castings*

Figures 9 through 12 present the simulation results obtained for an axisymmetric casting. The Al-7 pct Si alloy was cast into a sand mold, and the initial temperatures of the metal and of the mold were 720 and 20 °C, respectively. The heat transfer coefficient between the metal and the mold was taken into account *via* the heat-link procedure described in Section II (h = 1000 W/m^{2}K in this particular case). The calculation was performed using the enmeshment shown in Figure 1 (1139 nodes). The time-steps were 1 and 0.005 seconds for the macroscopic and the microscopic calculations, respectively. The growth law of the dendrite tips is still given by Eq. [17], and the parameters of the gaussian nucleation distribution are listed in Table I. Figure 9 shows the temperature field 50 seconds after pouring. Cooling curves, corresponding to the four locations labeled on Figure 1,

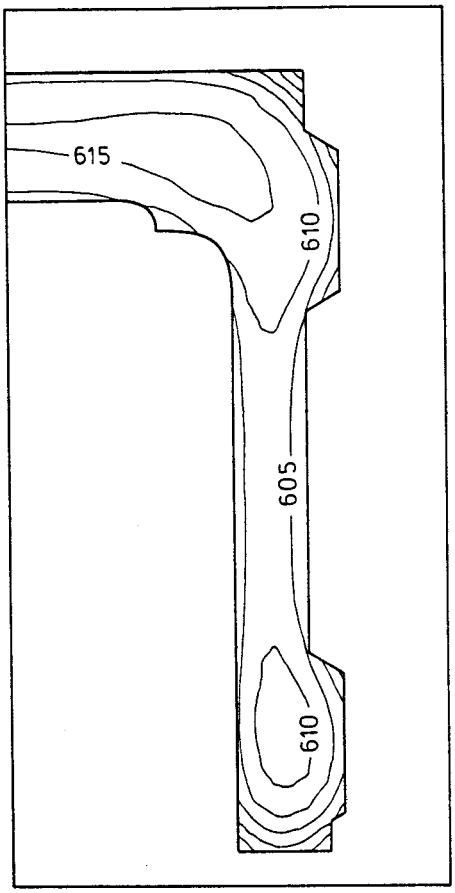

Fig. 9—Calculated temperature distribution within the casting (50 s after pouring) shown in Fig. 1 (Al-7 pct Si alloy). The temperature difference between the isotherms is 5 °C.

are plotted in Figure 10. As can be seen, each of these cooling curves exhibits a recalescence, calculated using the micro/macroscopic model. The maximum undercooling, ΔT_{max}, measured on these curves is the temperature difference between the liquidus temperature

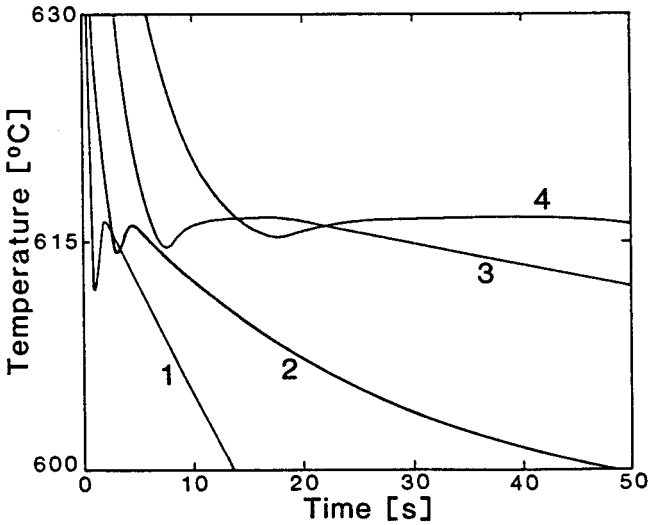

Fig. 10—Cooling curves calculated, using the micro/macroscopic model, at the mesh points shown in Fig. 1. Each of these curves exhibits a recalescence with a depth, ΔT_{max}, measured from the equilibrium liquidus temperature.

(T_{liq} = 618 °C for Al-7 pct Si) and the local minimum in the cooling curve near to recalescence.* Figure 11 shows a map of this maximum undercooling, ΔT_{max}, in the casting. In this case, ΔT_{max} varies from 2 °C at the center to 4 °C at the surface of the testpiece. As expected from experiments, the undercooling is lower in the center of the casting (*i.e.*, where the cooling rate is the lowest) than at the surface.

*Note that ΔT_{max} is not the difference between the local minimum and the local maximum of the cooling curve, which is often considered in industry to be the maximum equiaxed undercooling.

As shown in the nucleation model (Section III–B), the grain density is related directly to the maximum undercooling, ΔT_{max}, *via* the nucleation distribution, and the calculated grain radii also are listed in Figure 11. In the center of the testpiece (point 4, Figure 1), the grain radius is slightly larger than 4 mm, whereas, for higher cooling rates near the surface, the radius is of the order of 0.5 mm.

The program, 3-MOS, can also predict other microstructural parameters. Figure 12 presents a map of the secondary arm spacing, λ_2, for the same testpiece. Although the program can predict the dendrite tip radius and the associated initial dendrite arm spacing, coarsening smoothes out any variation in the initial dendrite arm spacing. Therefore, the values of λ_2 shown in Figure 12 were deduced from the standard coarsening model of Feurer and Wunderlin:[27]

$$\lambda_2 = M \cdot t_s^{1/3} \qquad [18]$$

where the coarsening rate constant, M, is given in Table I, and t_s is the local solidification time.

In order to test the validity of the model, various cases were calculated, with several initial and boundary conditions and different nucleation parameters. The observed behavior of the calculated cases always corresponded to that expected on the basis of experimental work. For example, the map of maximum undercooling (or grain radius) has been calculated for the same testpiece as that shown in Figure 1 but with different nucleation parameters. Decreasing the density of inoculant sites by a factor of 100, while keeping other parameters constant, increases the maximum undercooling (*i.e.*, the recalescences are deeper), together with the average grain radii. This behavior would correspond, for instance, to a noninoculated melt.

The same micro/macroscopic coupling was also applied to irregular eutectic alloys such as gray cast iron solidifying with an equiaxed morphology, by simply setting the internal solid fraction, f_i, in Eq. [10] equal to 1 and by taking account of the kinetics of the eutectic front. Since the diffusion layer around the grain envelope is much smaller than the grain radius in this case, grain

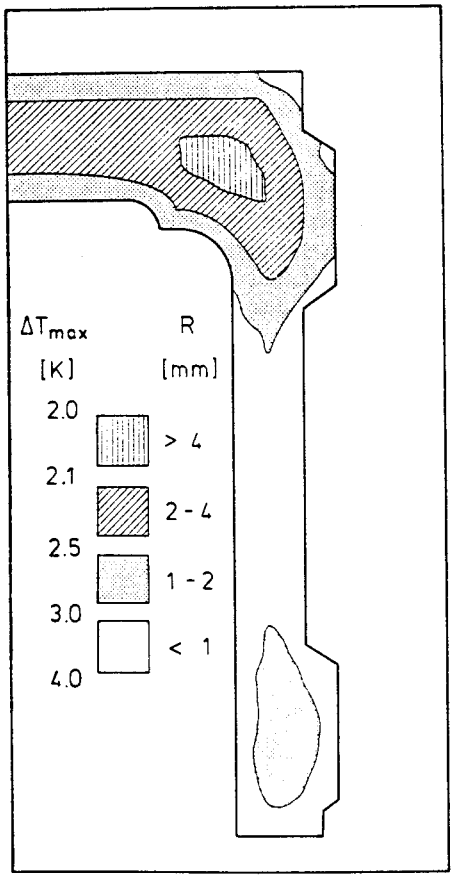

Fig. 11—Map of calculated maximum undercooling, ΔT_{max}, within the casting shown in Fig. 1. As ΔT_{max} can be related directly to the average grain size using the nucleation law (Fig. 2 and parameters listed in Table I), this figure also maps the average grain size, R_{av}, within the casting.

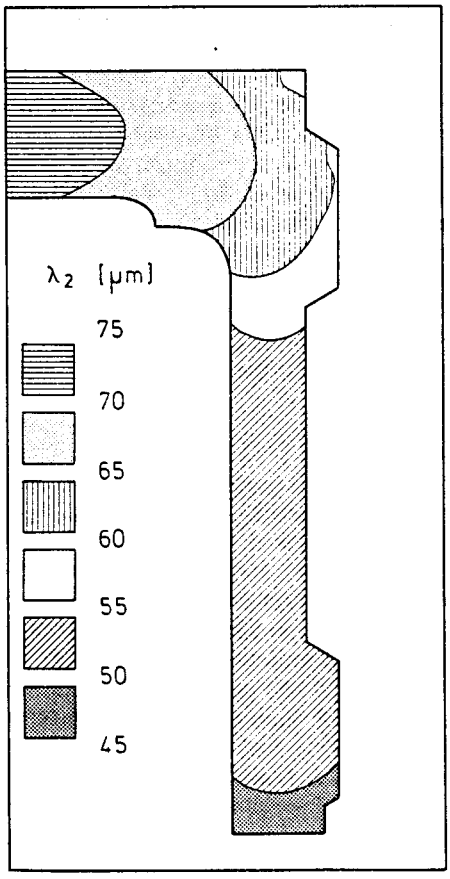

Fig. 12—Map of calculated secondary arm spacing, λ_2, within the casting shown in Fig. 1.

interaction was allowed for by considering the impingement of densely packed solid spheres.[23]

VI. CONCLUSION

A new and general approach to the modeling of equiaxed dendritic and eutectic microstructure formation in castings is proposed. At the macroscopic level, the heat diffusion equation is solved using an enthalpy formulation and a FEM implicit scheme. At the microscopic level, the nucleation and growth of equiaxed crystals is calculated at each node and time-step, knowing the variation in enthalpy deduced from the macroscopic calculation. In addition to the temperature field, solid fraction distribution, and parameters deduced from the isotherms evolution, the micro/macroscopic calculation provides interesting results concerning equiaxed microstructures, such as undercooling, grain size, fraction of eutectic, and microstructural spacings.

The results presented are for one-dimensional and axisymmetric geometries. Quantitative agreement between the measured and calculated recalescences and grain size has been demonstrated for one-dimensional castings of Al-7 pct Si. The behavior of the calculated cases for more complex geometries is in good qualitative agreement with that found in experiments.

The main advantage of the micro/macroscopic enthalpy-based model is the two time-steps procedure. First, this coupling permits us to avoid bouncing effects and reheating of meshes which leads to a good convergence of the results. Second, it dramatically reduces the computing time, thus permitting the application of the model to two- or even three-dimensional geometries.

As far as computing time is concerned, three different methods of calculation can be compared: (a) a standard macroscopic calculation of heat flow using the enthalpy formulation, Δt = 1 second; (b) a micro/macroscopic calculation using a single time-step procedure, $\Delta t = \delta t$ = 0.01 second; and (c) a micro/macroscopic calculation with two time-steps, Δt = 1 second and δt = 0.01 second. The time-step, Δt, of method (b) must be taken equal to δt, so as to describe recalescence with the same accuracy as that in scheme (c). (Method (b) will give rise to bouncing effects in most cases.) The CPU times for methods (a), (b), and (c) for the calculation of the axisymmetric test-piece shown in Figure 1 are listed in Table II. It can be seen that the two time-steps procedure (method (c)) increases only slightly the overall computing time with respect to the standard macroscopic calculation (method (a)), whereas the difference between methods (a) and (b) is very large. This can be understood easily since the macroscopic calculation of heat flow has to be done at each time step, δt, in this case.

The main problem in the practical use of the model is the correct choice of the two time-steps. As the macroscopic calculation is done implicitly, no Fourier criterion has to be satisfied. Thus, the two time-steps can be chosen freely within the limits shown in Figure 6(b). The macroscopic time-step has to be sufficiently large with respect to the recalescence time to avoid reheating of the meshes (bouncing effects) and be small enough to reduce the error associated with the linearization scheme of the heat flow equation (numerical diffusion). The choice of the time-step used in the microscopic calculation is easier; the maximum limit is dictated by the width of the recalescence, and there is no minimum limit. Further investigations will be made in this field in order to predict the best time-steps and mesh sizes as a function of each problem and to implement an automatic dynamic time-stepping procedure.

Table II. Computing Time for One Second of Solidification on Apollo DN3000 (1139 Nodes)

Method (a)	
Pure macroscopic calculation (1 step = 1 second)	180 [seconds]
Method (b)	
Micro/macroscopic calculation with a single time-step (100 time-steps = 1 second)	20,000 [seconds]
Method (c)	
Micro/macroscopic calculation with two time-steps (1 step macro = 1 second and 1 step micro = 0.01 second)	
(maximum CPU-time for one macroscopic time-step)	250 [seconds]
(average CPU-time per macroscopic time-step)	200 [seconds]

ACKNOWLEDGMENTS

The authors would like to thank Dr. J.P. Gabathuler of Schweizerische Aluminium AG for his invaluable help in performing the experiments. They also thank Professor H.E. Exner and Dr. J. Paul of the MPI-Stuttgart, their European partner within the COST program, for their painstaking quantitative metallographic measurements.

REFERENCES

1. W.D. Murray and F. Landis: *Trans. ASME*, May 1959, pp. 106-12.
2. P.R. Sahm and P.N. Hansen: *Numerical Simulation and Modeling of Casting and Solidification Processes for Foundry and Cast House*, Comité International des Associations Techniques de Fonderie, 1984.
3. W.S. Hwang and R.A. Stoehr: *J. of Metals*, 1983, vol. 10, pp. 22-29.
4. S.D. Ridder, S. Kou, and R. Mehrabian: *Metall. Trans. B*, 1981, vol. 12B, pp. 435-47.
5. V.R. Voller: in *Numerical Methods in Thermal Problems*, R.W. Lewis, K. Morgan, and W.G. Habashi, eds., Pineridge Press, Swansea, 1987, vol. V, pp. 693-704.
6. W. Oldfield: *ASM Transaction*, 1966, vol. 59, pp. 945-61.
7. D.M. Stefanescu and C. Kanetkar: in *Computer Simulation of Microstructural Evolution*, D.J. Srolovitz, ed., TMS-AIME, 1986, pp. 171-88.
8. I.L. Svensson and E. Lundback: in *State of the Art of Computer Simulation of Casting and Solidification Processes*, Proc. E-MRS Conference, H. Fredriksson, ed., Les Editions de Physique, Strasbourg, 1986, pp. 57-64.
9. K.C. Su, I. Ohnaka, I. Yamauchi, and T. Fukusako: in *The Physical Metallurgy of Cast Iron*, H. Fredriksson and M. Hillert, eds., North-Holland, 1985, pp. 181-89.
10. I. Maxwell and A. Hellawell: *Acta Metall.*, 1975, vol. 23, pp. 229-37.
11. I. Dustin and W. Kurz: *Z. Metallkunde*, 1986, vol. 77, pp. 265-73.
12. J.D. Hunt: *Mater. Sci. Engineer.*, 1984, vol. 65, pp. 75-83.
13. S.C. Flood and J.D. Hunt: *J. Cryst. Growth*, 1987, vol. 82, pp. 543-60.

14. J.L. Desbiolles, M. Rappaz, J.J. Droux, and J. Rappaz: in *State of the Art of Computer Simulation of Casting and Solidification Processes*, Proc. E-MRS Conference, H. Fredriksson, ed., Les Editions de Physique, Strasbourg, 1986, pp. 49-55.
15. Ph. Thévoz: Sc. Dr. Thesis No. 765, Swiss Federal Inst. Tech., Lausanne, 1988.
16. M. Rappaz and Ph. Thévoz: *Acta Metall.*, 1987, vol. 35, pp. 1487-97.
17. M. Rappaz and Ph. Thévoz: *Acta Metall.*, 1987, vol. 35, pp. 2929-33.
18. W. Kurz and D.J. Fisher: *Fundamentals of Solidification*, Trans. Tech. Publ., Aedermannsdorf, Switzerland, 1984.
19. M. Bernadou: MODULEF, *Une bibliothèque modulaire d'éléments finis*, Institut National de Recherche en Informatique et Automatique, Paris, 1985.
20. J.L. Desbiolles, J.J. Droux, J. Rappaz, and M. Rappaz: *Computer Phys. Rep.*, 1987, vol. 6, pp. 371-83.
21. D. Turnbull: *J. Chem. Phys.*, 1950, vol. 18, pp. 198-203.
22. B. Cantor and R.D. Doherty: *Acta Metall.*, 1979, vol. 27, pp. 33-46.
23. M. Rappaz, Ph. Thévoz, Z. Jie, J.-P. Gabathuler, and H. Lindscheid: in *State of the Art of Computer Simulation of Casting and Solidification Processes*, Proc. E-MRS Conference, H. Fredriksson, ed., Les Editions de Physique, Strasbourg, 1986, pp. 277-84.
24. J. Lipton, M.E. Glicksman, and W. Kurz: *Metall. Trans. A*, 1987, vol. 18A, pp. 341-45.
25. V.R. Voller, M. Cross, and P.G. Walton: in *Numerical Methods in Thermal Problems*, R.W. Lewis and K. Morgan, eds., Pineridge Press, Swansea, U.K., 1979, pp. 172-82.
26. E.E. Underwood: *Quantitative Stereology*, Addison-Wesley, Reading, MA, 1970.
27. U. Feurer and R. Wunderlin: *Deutsche Gesellschaft für Metallkunde*, Oberursel, DGM Fachbericht 38/677/x, 1976.